ELSEVIER

PII: S0032-3861(98)00025-1

Polymer Vol. 39 No. 23, pp. 5587–5599, 1998
0032-3861/98/$ – see front matter

The use of transmission electron microscopy to study the blend morphology of starch/poly(ethylene-*co*-vinyl alcohol) thermoplastics

Stephanie Simmons† and Edwin L. Thomas*
Program in Polymer Science and Technology, Department of Chemical Engineering, Department of Materials Science and Engineering, Massachusetts Institute of Technology, Cambridge, MA 02139, USA
(Received 19 June 1997; revised 8 December 1997; accepted 16 December 1997)

Transmission electron microscopy (TEM) was used to examine the morphology of extruded thermoplastic starch/poly(ethylene-vinyl alcohol) (EVOH) blends. Both the starch and EVOH polymers were found to be very beam sensitive: the maximum allowable beam dosages for the crystalline fraction of both components are estimated at less than 3.5×10^{-3} C cm^{-2} at 200 kV and room temperature. In addition, both polymers experienced significant mass thickness contrast variations which at moderate beam dosage ($> 6.0 \times 10^{-3}$ C cm^{-2}) led to contrast-reversal of images of the blend morphology. Noting the effect of the electron beam on the materials, low dose techniques were used with conventional TEM to reliably image the blends. For as-processed starch/EVOH blends, EVOH was observed to be the matrix component even at very high starch concentrations (up to 70%). Domain sizes of starch were observed to range from less than 0.1 μm to greater than 3 μm indicating that all of the starches became destructurized during the preparation of the blends. Variation in the blend structure was also observed at similar starch compositions (50%) for the three corn starch types. An analysis of contrast differences in blends containing Waxy Maize, Native Corn, and high amylose Hylon VII starches with EVOH suggested increasing miscibility with increasing amylose content in the starch component. Finally, structural gradients in thermoplastically formed articles (e.g. a starch/EVOH melt-spun fibre) were observed. © 1998 Published by Elsevier Science Ltd. All rights reserved.

(Keywords: blend morphology; electron microscopy; starch/poly(ethylene-vinyl alcohol) blends)

INTRODUCTION

The key to understanding both the flow characteristics and physical properties of polymer blends is the determination of their morphology. The polymer morphologist usually seeks to determine the number and volume fraction of certain phases at a given blend composition, to gain information on the domain size, shape, and connectivity of these phases, and to detect if and where crystallization and molecular orientation in a blend are occurring. Transmission electron microscopy (TEM) can be an especially useful technique to the researcher since one can view sub-micron scale domains without the removal of sample components by utilizing mass thickness, diffraction, and phase contrast differences within the specimen. One can also examine crystalline regions by performing electron diffraction on selected areas and by operating the microscope in dark field mode. In addition, the microscopist can observe gradients in structure from the surface to interior regions of a bulk sample by examining specimen cross-sections in TEM.

Despite these advantages of TEM, obtaining meaningful results often provides a challenge due to the difficulty in obtaining thin specimens with sufficient contrast, in overcoming the radiation sensitivity of the polymer samples, and in interpreting images taken under specific electron optical conditions[1]. In this paper, we give details on the use of transmission electron microscopy to investigate the microstructure of polymer blends that consist of thermoplastic starch and poly(ethylene-vinyl alcohol). Because of the difficulty in preparing microtomed samples, staining components preferentially, and imaging these systems in TEM, past use of this technique in examining thermoplastic starch-based blends has been very limited[2].

Starch, processed thermoplastically, can be employed as a biodegradable alternative in certain polymer applications (e.g. disposable packaging, cups, utensils, composting bags, etc.). Thermoplastic starch refers to granular starch which has been 'destructurized'[3,4] forming a mixture of its polymer constituents (amylose and amylopectin) and the various proteins, lipids, and smaller molecules (such as water) that are also contained in the starch granule. To attain better processability and to increase the level of mechanical stability and moisture resistance in the final product, starch is often extrusion blended with another polymer component, in our particular case, with poly(ethylene-vinyl alcohol) (EVOH) and with plasticizers such as glycerin and water. The composition of these blends can be tailored to yield the required flow and physical properties necessary for further thermoplastic processing such as injection moulding, fibre spinning, or film blowing.

Previous studies using scanning electron microscopy (SEM) provided general information about the bulk phase structure in extrusion blended starch–EVOH materials in

* To whom correspondence should be addressed. Tel.: (617) 253-6901; fax: (617) 258-7874; e-mail: elt@mit.edu
† Present address: Candescent Technologies Corporation, 6580 Via del Oro, San Jose, CA 95119, USA

which accessible starch-rich phase domains had been removed[2]. The extent of structural information attainable with SEM on these blends was quite limited due to the varied susceptibility of different starch types to the enzyme etchant. Also, the addition of an aqueous carrier for the etchant causes swelling and deformation of the blend as it is etched, probably changing the overall morphology. Others have used light microscopy to image starch–EVOH blends[5], however, the domain sizes observed are roughly the size of native starch granules ($\sim$10–25 μm).

TEM has been used to investigate the structure of granular starch, starch gels, and single crystals of amylose complexes, but only a few studies have focused on thermoplastic starch or starch-based blends. In the past, emphasis has been placed on investigating the structural components of native granules[6–9]. Because of the similarity of amylose and amylopectin in chemical composition and electron density, differentiation between these components is not easily achieved in TEM (in fact, no differentiation between the two polymers in the microstructure of starch gels has been observed[10]). The internal structure of starch granules is revealed only through a complex and lengthy series of dehydrating, embedding, sectioning, chemical treating, and staining or shadowing steps which often produce artifacts that limit the interpretability of transmission electron micrographs[7]. Such structural development studies examined the growth rings of various types of starches by methods such as staining with potassium permanganate, enzymatically treating with α-amylase, partially degrading by acid treatment (linterization), and/or shadowing with metals[11–14]. A study performed by Kassenbeck successfully revealed the fine structure of wheat and maize starches by using periodate, thiosemicarbazide, silver nitrate, and osmium tetroxide staining agents to distinguish the crystalline from non-crystalline regions in the starch granules[15,16]. Kassenbeck established that amylose is essentially located in the nucleus of the granule and is surrounded by growth rings formed by amylopectin chains which undergo crystallization into alternating radial layers approximately 60 Å thick (i.e. the rasemose model). A summary of the extensive and varied specimen preparation techniques for studying the native starch granules by TEM is given by Gallant and Sterling[17] and Blanshard[18].

The often ambiguous results of these initial studies (attributed mostly to granule folding during sample preparation) were later overcome by an embedding and microtoming procedure developed by Chanzy et al.[19]. Granule sections were observed under frozen hydrated conditions by TEM in diffraction mode[19]. Without staining, the presence and location of granules in TEM could only be determined by supplementing the electron diffraction results with optical micrographs (taken with polarized light) of the same sample region. The location of the starch granules became evident from 'Maltese-Cross' patterns which resulted from the predominantly radial orientation of the polymer chains within the granule[20]. The electron diffraction patterns of these potato starch samples were typical of B type starch and exhibited fibre diffraction patterns for the central sections and strongly arced or continuous ring diagrams for non-central or tangential sections of the granule[19]. Further electron diffraction studies have been performed by Chanzy's group and others on single crystals of amylose[21,22] and amylose acetate[23].

In the present study, TEM is performed on biodegradable blend materials produced from the thermoplastic processing of starch in which the ordered granular structure has been partially or totally eliminated. We seek to image the microstructure that results from the extrusion blending, fibre spinning, film blowing, and injection moulding of three varieties of corn starch (differing in amylose/amylopectin ratio) with another polymer, poly(ethylene-vinyl alcohol). Since there have been very few studies published which utilize TEM on thermoplastic starch-based systems[10,24], and none in particular on starch/poly(ethylene-vinyl alcohol) systems, emphasis is placed on the experimental details of imaging such systems in this paper. The structural information on these blends gained from TEM is put in context with other structural and processing studies and is presented separately[2,25].

Due to the moisture sensitivity of starch and the presence of plasticizers in the blend, special steps are taken during the microtoming and sample preparation process. Next, the beam sensitivity of both starch and EVOH is established in TEM, and imaging conditions that will minimize damage of the sample as it is exposed to the electron beam are prescribed. Contrast mechanisms, which include mass thickness, diffraction and phase contrast, between starch and EVOH-rich domains are considered as well as the effect of partial blend miscibility on the observed structures. The choice of a selective stain to enhance contrast between the starch and poly(ethylene-vinyl alcohol) components, both of which are very similar in their chemical composition, is addressed. Structural changes which occur in the blends as they are imaged using the electron microscope are then established. Finally, having obtained a reliable method of preparing and then imaging starch/poly(ethylene-vinyl alcohol) blends, we present their morphologies as a function of composition, compare the morphology of different starch varieties in blends with EVOH, and observe the blend structure that arises at the near surface region of a melt-spun starch/EVOH fibre.

EXPERIMENTAL

Materials

Three types of corn starch, varying in amylose/amylopectin ratio, were extrusion compounded with poly(ethylene-vinyl alcohol) in order to explore processability, physical property, and morphological changes of these blends as a function of composition. Each starch was blended in varying proportions with the poly(ethylene-vinyl alcohol) using a Leistriz (34 mm) twin screw extruder (Novon Research Division, Warner-Lambert, Morris Plains, NJ) under shear, heat, and moisture conditions[2,26] that would ensure starch granular destructurization[3]. Specific details on the compounding of these blends is given in previous work[2,25].

Amioca Waxy Maize (WM, 100% amylopectin), Melojel Native Corn starch (NC, 72% amylopectin), and Hylon VII (HY) a high-amylose starch, were obtained from National Starch and Chemical Co. (Bridgewater, NJ). Naturally occurring triglyceride additives were pre-mixed with the starch fraction in small amounts (3 wt.% to the starch fraction) to aid in processing. Poly (ethylene-vinyl alcohol) (EVALCA E105A), containing 56 mol.% vinyl alcohol groups, was supplied by EVALCA Co. (Lisle, IL). Glycerin (15% by weight of the total feed) was injected into the extruder during processing. During the compounding of certain blends, a small quantity of water (not more than 10%) was added to reduce problems with torque build-up in the extruder; water vapour was subsequently vented near the

extruder exit. Moisture content at the extruder exit was measured by titration to range from 1.4 to 15.8% depending upon starch type and composition[2]. Nomenclature of each blend is presented as 'starch type:percent of starch' (i.e. NC30 refers to a blend containing a 30:70 ratio by weight of Melojel Native Corn starch to EVOH).

We sought to characterize these materials as polymer–polymer blends (i.e. starch-rich or EVOH-rich domains). However, given the complex nature of these materials (i.e. three polymer components which are each crystallizable, two plasticizers, and various small molecules), we must take into account the effect of plasticizers and various small molecule additives in addition to the likely presence of orientation from processing in analyzing the overall morphology. For this reason, blends containing only starch or only EVOH with plasticizer (*vic*. glycerin and water) were examined first to determine structural features observable in either polymer. Next, blends of starch with EVOH were examined.

Sample preparation

Bulk polymer samples require microtoming into sections that are sufficiently thin so that the electron beam can pass through the specimen thus forming an image in the TEM[27]. For polymer–polymer blends, the shape, size, and distribution of the polymer phases also define limits to the specimen thickness. Ideally, specimens should be thinner than the thickness of the phase domains one seeks to image and there should be no overlapping of domains in projection. Otherwise, only uncorrelated fluctuations in the observed projected images are detected and valid dimensions of individual domains cannot be readily discerned (such as for the case of a large volume fraction ($>$ 30%) of randomly distributed domains which are small in comparison to the specimen thickness[28]).

A Reichert-Jung FC4E cryo-ultramicrotome was employed for preparing sections using a sample temperature setting of -20 to 15°C and a knife temperature from -20 to 0°C. Cutting temperatures were optimized with respect to the mechanical characteristics of each blend; usually, specimen and knife temperatures decreased as the EVOH level increased. For starch, T_g is a strong function of the relative humidity at which it is stored and can range from below room temperature to greater than 200°C[29]. For pure EVOH, T_g occurs at 55°C. The presence of glycerin and water in the blends will serve to lower these transition temperatures. Moreover, the small molecule components may partition unevenly between the polymeric components. An accurate determination of the glass transition temperatures for the blends via differential scanning calorimetry was difficult due to the low signal to noise of the T_g transition and the overlapping temperatures of multiple endothermic transitions for the blends[2]. However, the range of -20 to 15°C was found to cause the least damage to blend specimens and it is estimated that the T_g values in the blends do not fall in this temperature range.

Samples were cut with a razor prior to placing them in the sample holder. A trapezoidal mesa ($<$ 0.2 mm per side) was trimmed with the microtome using a glass knife following procedures detailed in the literature[30]. A 35° diamond (Diatome®) knife was used to cut sections using the microtome setting of 30–50 nm. Samples were carefully collected from the knife with an eyelash tool and deposited onto a droplet of ethanol placed on a either a 400 or 600 mesh copper grid (Ted Pella, Inc., Redding, CA). The grids were blotted on filter paper to remove any excess ethanol. It must be stressed that no water was used during the microtoming process to eliminate swelling of the starch fraction (ethanol showed no interaction with any of the starch blends). Grids containing sample sections were placed overnight in a desiccator containing 8 mesh anhydrous calcium sulfate (W. A. Hammond Drierite Co., Xenia, OH). Prior to viewing in TEM, certain sections were placed in a stainer containing elemental iodine (Mallinckrodt Specialty Chemicals) and exposed to iodine vapour for 1 h to preferentially stain the amorphous starch-rich fraction. In addition, certain sections were coated with a thin layer of carbon ($<$ 50 Å) using a Ladd vacuum evaporator (Ladd Research Industries, Inc., Burlington, VT) to improve the electrical and thermal conductivity as well as the rigidity of the sections in the TEM.

Instrumentation

A JEOL 200 CX TEMSCAN electron microscope equipped with a tungsten filament source was employed at 100–200 keV to image the samples. The spherical aberration coefficient and focal length of the objective lens were 6.7 mm and 5.0 mm, respectively. Objective apertures of 20 and 40 μm diameters, corresponding to 0.10 and 0.17 Å^{-1} cut off values in reciprocal space were most often employed. Because of the sensitivity of both starch and EVOH to the electron beam, samples were imaged using low dose techniques and employing a small condenser aperture (200 μm) and small spot size[8,12,31–33]. Images were obtained at relatively low magnification (5–10 k×) by first focusing on an area, translating to an adjacent area, and recording a 2–4 s exposure with Kodak SO-163 image plates.

Image analysis

Selected negatives were digitized using a UMAX UC630 scanner with transparency attachment. Adobe Photoshop® (version 2.5 LE) was used for digitizing the images at 300 or 600 dpi over a range of grey scales from 0 to 255 (0, black; 255, white). Optical densities corresponding to measured grey scales were obtained through calibration of the scanner with a Kodak Q-14 Gray Scale (20 density steps at 0.1 density increments). Digitized images were saved as TIFF files which were imported into the NIH Image program (Version 1.35) for analysis of domain size and intensity. Intensity profile plots were determined from various micrographs to quantify image contrast and its dependence on microscope operating conditions and on beam damage.

RESULTS AND DISCUSSION

The observation of a starch/poly(ethylene-vinyl alcohol) blend in the TEM is not as trivial as for a simple binary blend system, for example, a polystyrene/polybutadiene blend in which one primarily uses mass thickness contrast to discern the relatively large ($>$ 1 μm) unstained polystyrene domains from polybutadiene domains heavily stained with osmium tetroxide. For this reason, we highlight the following issues involved in the imaging of starch/EVOH blends: (1) the beam sensitivity of both starch and poly(ethylene-vinyl alcohol), (2) the contrast mechanisms involved in discerning starch from EVOH domains, and (3) contrast changes as a function of electron beam exposure. These issues are important to the interpretation of blend morphology as a function of blend composition, of starch-type, and of subsequent thermoplastic processing (e.g. melt fibre spinning).

Beam sensitivity of starch and EVOH

Organic materials undergo radiation damage when exposed to the electron beam. The degree of damage is related to the total dose, D, the product of beam current density, j (A cm^{-2}), and irradiation time, t [34]. For polymers, the main effects of radiation damage are cross-linking and chain scission. Both occurrences generally result in loss of mass through the production of volatile components (e.g. H_2, CH_4, CO, CO_2, H_2O). The geometry of the sample and the cross-section of the electron beam, in combination with the beam intensity, will also cause changes in the specimen due to secondary thermal effects (e.g. loss of crystallinity, desorption of substances such as water, and decomposition), charging effects with strong electric fields (e.g. specimen motion and curling of sections) as well as dimensional changes due to crosslinking.

In order to understand the effect of beam damage on the starch/EVOH blends, TEM was performed on the HY100 and the EVOH/GLY blends. This initial study was performed to gain information about the crystalline nature of each blending component and the nature of beam damage. It should be noted that a starch/EVOH blend does not represent a superposition of the two pure components since different partitioning of plasticizers (i.e. glycerin, water) and some polymer–polymer mixing may occur. *Figure 1a* depicts the morphology of unstained HY100 as imaged under low dose conditions using an estimated electron dose of approximately 9×10^{-4} C cm^{-2}. *Figure 1b* shows the influence of beam damage on the sample which has been exposed to the beam for an additional 20 s. With increasing electron dose, the HY100 shows significant dimensional changes including the enlargement of voids, mass loss, and the formation of a rippled texture. The lighter oblong areas, with major axes approximately 0.1–0.2 μm in size, which are observed in *Figure 1a*, are barely visible in the beam damaged sample. The diffraction pattern for the HY100 blend was difficult to record due to the multiple scattering from the specimen and the limited amount of crystallinity present which will lower the extent of diffraction contrast attainable from this sample[2]. Faint rings corresponding to a V-amylose complex were nevertheless visible providing evidence for crystallinity (see inset of *Figure 1a*). At the operating voltage of 200 keV, the electron beam lifetime of the V-amylose crystals in HY100 was estimated to be no more than a quarter of that of stretch-oriented PE film (an accurate value was difficult to determine), and, therefore, the maximum allowable beam dosage for V-amylose crystals is estimated to be less than 3×10^{-3} C cm^{-2} (based on the total end point dose for polyethylene crystals at 200 keV and 20°C).

A different beam damaged morphology was observed for EVOH (see *Figure 2*). Initially appearing as a relatively homogeneous material (*Figure 2a*), the EVOH/GLY blend developed a mottled texture as the sample became damaged (*Figure 2b*). The ring-like domains (~1 μm in size) which form may indicate the out of plane buckling of small EVOH spherulites due to beam effects[35]. A banded spherulitic texture as observed in more typical semi-crystalline polymers was not observed for the EVOH/GLY material. Crystallinity, however, was readily apparent in the diffraction pattern (see inset of *Figure 2a*) and corresponds to X-ray diffraction data[2,25]. The crystal lifetime for EVOH containing 44 mol.% vinyl content was easier to measure

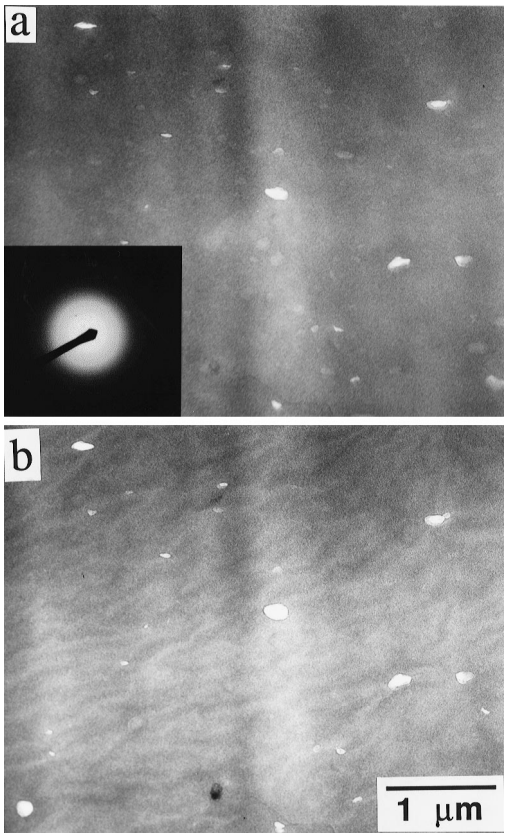

Figure 1 Bright field micrographs of the HY100 blend (Hylon VII high amylose starch compounded with glycerin and water). (a) The morphology and electron diffraction pattern observed under low dose conditions (D~9×10^{-4} C cm^{-2}). (b) The same region after 20 s total exposure to the electron beam (D~3.5×10^{-3} C cm^{-2})

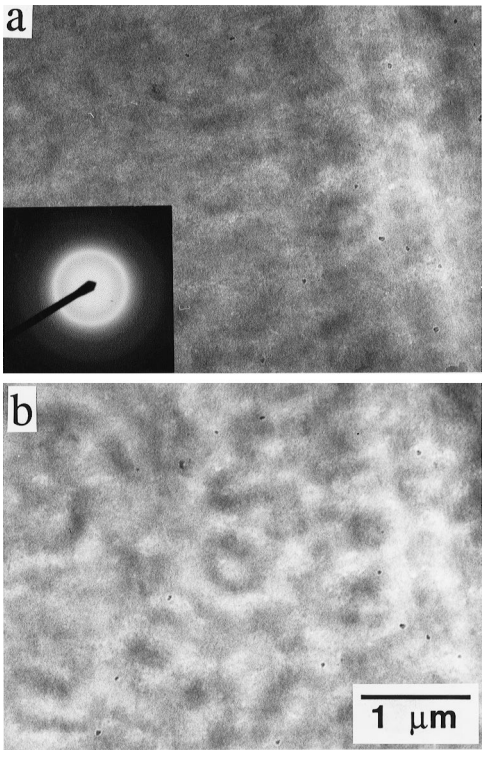

Figure 2 Bright field micrographs showing a microtomed section of the EVOH/GLY blend (EVOH compounded with glycerin). (a) The morphology and electron diffraction pattern observed under low dose conditions (D~9×10^{-4} C cm^{-2}). (b) The same region after 20 s total exposure to the electron beam (D~3.5×10^{-3} C cm^{-2})

than for the starch and corresponded to a somewhat higher maximum allowable beam dosage, $\sim 3.5 \times 10^{-3}$ C cm^{-2}.

The observed morphology of both starch and EVOH is thus highly dependent upon the amount of beam dose that each receives (i.e. both components are very sensitive to the electron beam). Studies by Reimer[34] showed that only 50% of the initial mass remained for starch and 50% of the original polyvinyl alcohol remained after long term electron irradiation at a current density of 0.3×10^{-6} A cm^{-2}. (In other words, electron beam damages principally through chain scission and crosslinking and results in mass loss up to 50% via irradiation for starch and polyvinyl alcohol.) Using a simple rule of mixtures, only 60% of the initial mass of EVOH containing 56% vinyl alcohol repeat units is expected to remain after long term electron beam exposure. For polyethylene, which retains 80% or more of its initial mass, mainly cross-linking occurs and mass loss is primarily attributed to the formation of H_2 gas[34]. For polymers containing alcohol groups, chain scission at the –COH residue is favoured and H_2, CO, and H_2O gases are formed[34]. Loss of crystallinity, cross-linking, and chain scission will result in both density and thickness variations in the polymers as they are imaged. The structural appearance of radiation sensitive polymer blends will change since the mass thickness contrast between phase domains is altered during TEM imaging. For this reason, micrographs depicting the starch/EVOH blend morphologies were taken under low dose conditions (i.e. 5–10 k× magnification with minimum beam exposure, $< 1 \times 10^{-3}$ C cm^{-2}) by focusing on an area, then translating to a previously unirradiated, adjacent area to take the exposure. In this way, structural changes to the specimen are minimized by operating the TEM under conditions that are below the maximum allowable beam dosage for starch and EVOH crystals ($< 3 \times 10^{-3}$ C cm^{-2}) and that will minimize the extent of beam damage that results in crosslinking and scission of the starch and EVOH polymer chains.

Contrast mechanisms

Contrast arises in TEM due to spatial variations in the phase and amplitude of the specimen transmission function, $\Psi(\mathbf{r})$, as incident electrons interact with the sample. Details on the image formation and contrast mechanisms using TEM can be found in various references in the literature[27,31,36,37]. In this section, we address contrast mechanisms and discuss the relevance of each type of contrast in interpreting TEM images of the starch/EVOH blends.

Amplitude contrast (mass thickness or diffraction contrast) results from loss of electrons by their scattering outside of the objective aperture. For non-crystalline samples that scatter incoherently in bright field (i.e. no diffraction contrast), mass thickness contrast arises from differences in the fraction of the incident beam intensity, I_o, which is collected by the objective aperture for different domains (which extend completely across the film thickness) of density, ρ, and thickness, t. This intensity, I, also depends on the optics through the choice of beam energy, E_o and objective aperture size, α, parameters which define the effective mass scattering cross-section, S_p. The value of I, at location i, is defined by:

$$I(E_o, \alpha)_i = I_o \, e^{-S_p(E_o, \alpha)\rho_i t_i} \tag{1}$$

The level of contrast, C, in bright field mode, resulting from mass thickness differences between two components at adjacent locations 1 and 2, can be expressed as (for I_1 greater than I_2):

$$C = \frac{I_1 - I_2}{I_1} = \frac{e^{-S_p\rho_1 t_1} - e^{-S_p\rho_2 t_2}}{e^{-S_p\rho_1 t_1}} \tag{2}$$

For S_p of approximately 3.5×10^{-3} m^2 mg^{-1} and a constant ($t_1 = t_2$) estimated thickness of 1000 Å, the initial contrast, C, between starch ($\rho \sim 1.45$ g cm^{-3}) and EVOH ($\rho \sim 1.15$ g cm^{-3}) is approximately 0.08, indicating that starch and EVOH-rich domains should be initially discernible via mass thickness differences. Image analysis performed on a near-focus image (where phase contrast of large scaled objects is minimized) of an unstained NC30 blend (30% native corn starch/70% EVOH), yielded a value for contrast of 0.05 between unstained starch-rich and EVOH-rich domains. This lower value of contrast may indicate partial miscibility between the starch and EVOH fractions which would result from a decrease in density for the starch-rich domains and a density increase in the EVOH-rich areas. A quantification of the level of miscibility between the starch and EVOH fractions by using measured contrast values was considered but not achieved to due the effects of beam damage on the samples.

Diffraction contrast results from scattering outside the objective aperture by crystalline regions which are properly oriented for diffraction. Diffraction contrast is often used to map out the displacement fields, defects, or textures present in crystalline samples (e.g. see Chacko *et al.*[38]). The diffracted intensity depends on the local deviations of the crystal lattice planes from the Bragg angle[27], as follows:

$$I(\boldsymbol{s}) \cong |F(hkl)|^2 \frac{\sin^2 \pi \boldsymbol{s} t}{\sin^2 \pi \boldsymbol{s}} \tag{3}$$

where $F(hkl)$ is the structure factor for the (hkl) reflection, t is the crystal thickness, and s is the deviation from the Bragg condition. The diffracted intensity falls off to zero at less than one degree of misorientation for crystals of thickness of approximately 100 Å. By employing an objective aperture with a cut off K_{MAX} diffraction contrast occurs in regions where the Bragg condition is satisfied and where $K > K_{MAX}$. Thus, in bright field mode, these regions appear darker in the TEM image than areas where $s \neq 0$ and/or $K < K_{MAX}$, since $I = I_o - I(s)$. When the objective aperture is set to collect electrons scattered under a certain Bragg condition (i.e. dark field mode), these imaged areas appear bright. Because of the relatively low levels of crystallinity in the EVOH and starch materials and the rapid loss of crystallinity due to electron exposure, diffraction contrast is not a significant contrast mechanism for the starch-EVOH systems.

Phase contrast depends on the phase shift of the transmitted wave which is a function of the electron microscope transfer function and the specimen transmission function, $\Psi(r)$[28,36,37]. In bright field, image phase contrast can be represented by the inverse Fourier transform of the product of the microscope transfer function, and the Fourier transform of the function, $\Psi(r)$, if we consider a weak phase object:

$$C_{phase} = \frac{I(\boldsymbol{r}) - I_{ave}}{I_{ave}} = F^{-1}[2A(\boldsymbol{K}) \sin \chi(\boldsymbol{K}) F\Psi(\boldsymbol{r})] \tag{4}$$

The electron microscope transfer function $A(\boldsymbol{K}) \sin \chi(\boldsymbol{K})$ modulates object frequencies in the image, where $A(\boldsymbol{K}) = 1/0$ inside/outside the objective aperture

and the $\boldsymbol{K}$-dependent phase shift is given by:

$$\chi(\boldsymbol{K}) = \pi\lambda(\Delta Z)\boldsymbol{K}^2 + \frac{\pi}{2}C_s\lambda^3\boldsymbol{K}^4 \quad (5)$$

ΔZ and C_s are the defocus and spherical aberration coefficients of the objective lens.

$\Psi(\boldsymbol{r})$ is proportional to the product of the mean inner potential, $\bar{\phi}(\boldsymbol{r})$, and the sample thickness:

$$\Psi(\boldsymbol{r}) = \frac{\pi}{\lambda V_o}t\bar{\phi}(\boldsymbol{r}) \quad (6)$$

where λ is the wavelength of the electron and V_o is the accelerating voltage. The mean inner potential, $\bar{\phi}$, can be estimated from the sample density, ρ, and f_i, the electron-scattering factor at zero angle of the ith atom of the basic structural unit of molecular weight, M:

$$\bar{\phi} = 69\ \frac{\rho}{M}\ \sum_i f_i \quad (7)$$

Using values of $f_H(0) = 0.221$, $f_C(0) = 1.024$, $f_O(0) = 0.840$ in p-units[39], the mean inner potential was calculated to be roughly 7.2–7.3 V for various types of starch ($\rho \sim 1.45$–1.47 g cm^{-3}, $M = 161$ g mol^{-1}, monomer units) and 7.3 V for EVOH (56 mol.% VOH, $\rho \sim 1.15$ g cm^{-3}, $M \sim 37$ g mol^{-1}, monomer units), respectively. The close similarity of the respective mean inner potentials indicates that one probably cannot discern between unstained starch and EVOH domains through phase contrast.

To illustrate the contrast mechanisms occurring between starch and EVOH, a through-focus series taken of a blend containing a native corn starch/EVOH ratio of 30:70 (NC30 blend) is shown in *Figure 3*. The minority component starch-rich domains appear dark in the micrograph against the lighter EVOH-rich matrix background. One should note that the near-focus image (*Figure 3b*) was taken first at an exposure of 4 s ($\sim 9.3 \times 10^{-4}$ C cm^{-2}), and beam damage is evident in the texture which has developed in the matrix. Subsequent beam damage occurs for the underfocus and overfocus images so the level of contrast is changing between domains and *Figure 3* should only serve to illustrate the primary mechanisms of contrast. The near-focus image shows definite contrast between darker, starch-rich domains, indicating that mass thickness contrast effects are primarily responsible for differences in the appearance of domains. The large underfocus ($\Delta Z \sim -13.6\ \mu$m) and large overfocus images ($\Delta Z \sim +13.6\ \mu$m) provide finer details from the phase contrast which arises from non-zero values of the microscope transfer function; negative values of defocus reinforce the mass thickness contrast whereas positive values oppose it. Defocusing reveals discernible microtome cutting lines, voids, and distinct domain boundaries (see *Figure 3a*).

At low to medium resolution, amplitude contrast generally dominates the overall image contrast with phase contrast providing finer details when defocusing the microscope[31]. The spatial frequency content of the NC30 sample is highly complex and starch-rich domains vary over the range from 0.1 to greater than 1 μm in size. Phase contrast may add definition to the observed image by highlighting differences that occur in the microtoming characteristics of each phase (at $\Delta Z \sim \pm 13.6$ mm), contrast is enhanced for lower frequency objects, $d > 0.08\ \mu$m). Although the sample is semi-crystalline, the measured and calculated densities of amorphous and crystalline EVOH at a composition which contains 56 mol% VOH are very similar (~ 1.15)[40]. Similar densities for thermoplastic starch and V-amylose crystals are also reported (~ 1.4 g cm^{-3})[41]. Based on mass thickness contrast, starch should appear darker taking into account density differences. However, beam damage which affects specimen composition, density and thickness, will influence values for the mean inner potential.

Staining of the starch-rich domains

To improve mass thickness contrast between the starch and EVOH domains it is desirable to use a specific heavy metal stain (so as to increase the electron density of one phase). Since starch and EVOH have essentially the same chemical constituents (both contain C–O, O–H, C–H, and C–C groups), finding a stain which would distinguish between the two components in TEM provided a challenge. Stains considered were osmium tetroxide (OsO_4), ruthenium tetroxide (RuO_4), uranyl acetate (UA), ruthenium red (RR), and iodine. Neither of the OsO_4 and UA stains react with polysaccharide chains specifically, and essentially concentrate into regions of high free volume. Uranyl acetate has been used in the past with some success in obtaining structural information through TEM of starch gels[42,43] and starch and starch blend thin sections in which the granule has not been completely destructurized[8,44]. Previous work has shown that ruthenium red, although it seems a prime candidate for polysaccharide staining[45], is unreactive with neutral polysaccharides[46]. Iodine is a well known positive stain for amylose and amylopectin, forming a complex

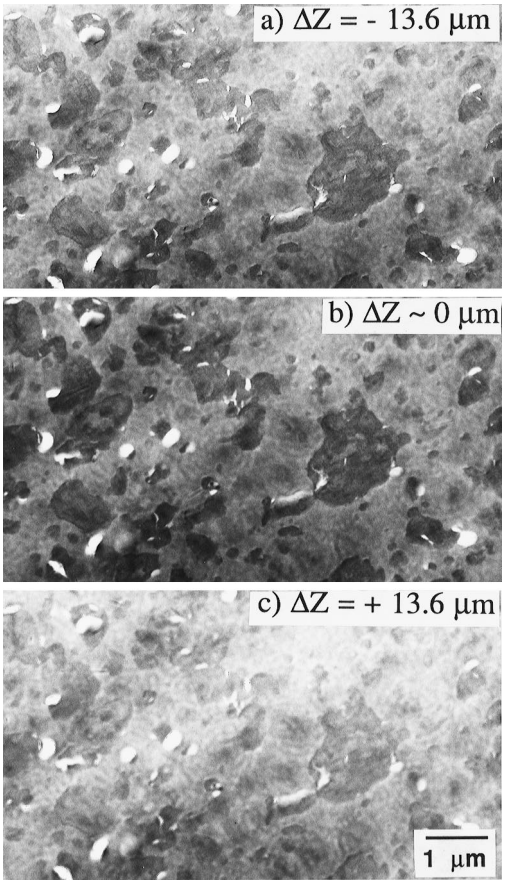

Figure 3 Through-focus series of a NC30 microtomed section (cut perpendicular to extrusion direction): (a) $\Delta Z \sim -13.6\ \mu$m, (b) near-focus, (c) $\Delta Z \sim +13.6\ \mu$m. Phase contrast arises as the microscope is defocused (a and c). Note that the sample undergoes beam damage during imaging (order of image taking and estimated total beam dosage: (b) $D \sim 9 \times 10^{-4}$ C cm^{-2}, (a) $D \sim 1.9 \times 10^{-3}$ C cm^{-2}, (c) $D \sim 2.8 \times 10^{-3}$ C cm^{-2})

within the helical starch polymer chains[20]. Samples were microtomed and stained with osmium tetroxide, ruthenium tetroxide, uranyl acetate, and ruthenium red, but no increased contrast between components was readily apparent. However, iodine was found to preferentially stain the starch-rich domains.

Iodine is known[47] to physically absorb into the amorphous regions of semi-crystalline polymers such as polyethylene. Iodine also forms chemical complexes by binding in linear sequences within the interiors of amylose, amylopectin, and poly(vinyl alcohol) helices[20,48–55]. Generally, this complexing behaviour occurs for starches that are not highly crystalline (i.e. already V-amylose complexed starches will not react with the iodine)[20]. Staining the bulk extrudate (pellets) for 4 h with iodine resulted in a colour change from translucent yellow to dark violet for thermoplastic starch pellets and only a slight change from clear to light yellow for the neat EVOH blend (indicating little to no complex formation in this component). The different staining behaviour provides a means for enhancing the mass thickness contrast between starch-rich and EVOH-rich regions. Any physisorbed iodine will desorb in the vacuum chamber of the electron microscope and in the electron beam due to the low pressure and possible sample heating[17]; complexed iodine will be less volatile, but as starch is irradiated it is likely that with the ensuing structural changes to the starch, the iodine stain will be lost. Again, low dose procedures are critical in obtaining useful information from TEM.

To confirm that the use of iodine promotes contrast between starch and EVOH, micrographs taken under similar conditions for unstained and stained NC30 sections were digitized and analyzed. For the unstained sample, the average contrast, *C*, was determined to be 0.05. For the stained sample, the average contrast increased to 0.11, indicating that the iodine stain is preferential to the starch-rich domains. Intensity profiles showing the effect of the iodine stain on the NC30 sample are shown in *Figure 4*. It should be noted that the iodine also penetrates the EVOH matrix, as evident in the overall shift to lower optical density of the negative (0.68), but it does not penetrate into the EVOH-rich matrix to the degree that it complexes with the starch.

Contrast changes as a function of beam dosage

Given the results of the beam sensitivity study performed on the neat starch and EVOH materials, we next determined the effect of beam dose on the structure of starch-EVOH blends. In *Figure 5*, a series of micrographs of the NC30 blend (previously stained for one hour with iodine) are displayed as a function of time at a specific beam current density ($\sim$2.3 A cm^{-2}). A line profile plot showing the changes in contrast as a function of beam dosage is shown in *Figure 6*.

Figure 5a depicts the initial structure of the NC30 blend at a defocus of $\sim$13.6 μm taken at a magnification of 5 k$\times$ and exposure time 4 s. Note, contrast is artificially enhanced with the use of high contrast, grade 4 print paper. The dark, starch-rich domains (less than 0.1–1.2 μm) are easily discernible against a grey background. Image contrast calculated from intensity analyses is 0.11. Holes and thin regions appearing bright in the micrographs are present either adjacent to or within the starch-rich domains. These areas may be attributed to microvoiding within the blend due to foaming of plasticizer (mainly water) during the extrusion blending process. Cracks observed within the starch-rich domains may have occurred during microtoming due to the brittle properties of the starch component. Microtome cutting lines are also visible. The matrix itself possesses a slightly mottled texture which could be due to

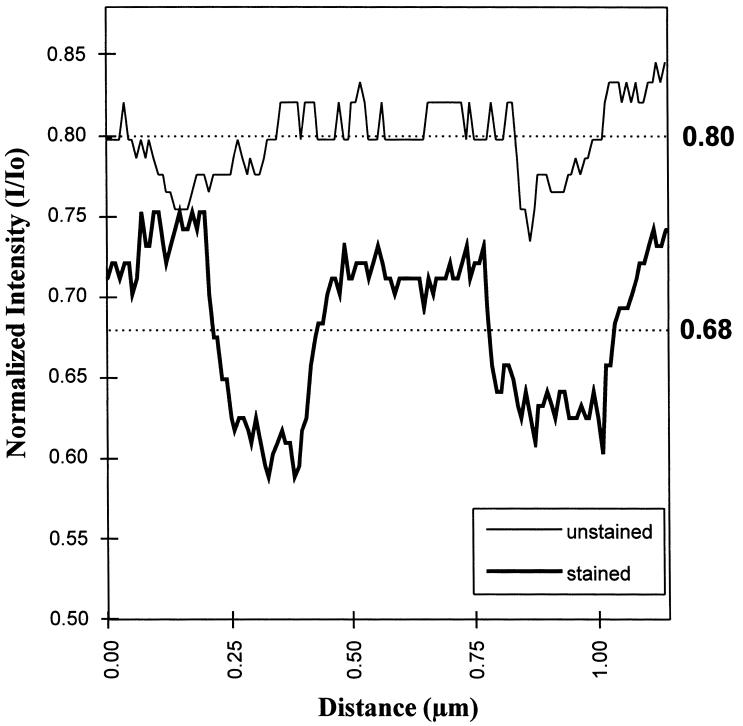

Figure 4 Comparison of intensity profiles obtained from micrographs taken under similar conditions (near-focus, 10 k$\times$, 4 s exposure, $D\sim9\times10^{-4}$ C cm^{-2}) for an unstained and iodine stained section of an NC30 blend. Contrast between the starch-rich domains (appearing at lower intensities than the EVOH matrix) increases from 0.05 to 0.11. Note also that the average intensity of the image, the optical density of the micrograph negative, decreases as it is stained (average intensity values are shown by the dashed line and at the right of the graph)

the presence of small starch-rich domains which are less than the thickness of the film or due to initial beam damage to the EVOH component. The following set of micrographs seem to indicate that the latter scenario is valid.

As the section is irradiated it undergoes mass loss such that the average measured intensity of the exposed film increases with beam exposure (i.e. I/I_o values are 0.70, 0.71, 0.74, 0.77). After 30 s beam exposure (*Figure 5b*), the NC30

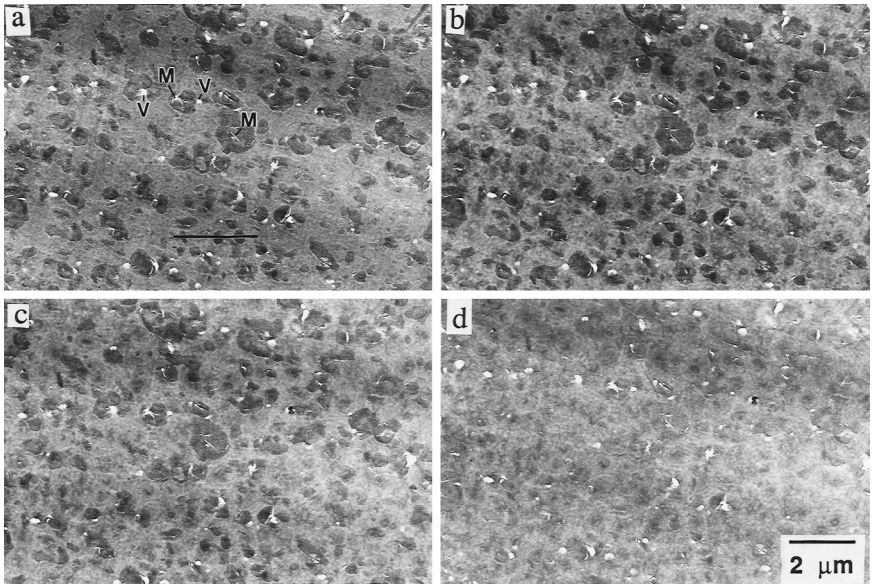

Figure 5 Bright field micrographs showing an iodine stained NC30 blend section as a function of time in the beam at a current density of approximately 2.3×10^{-4} A cm^{-2} (at 5 k×): (a) initial exposure, $t = 4$ s, $D \sim 9.3 \times 10^{-4}$ C cm^{-2}; (b) $t = 34$ s, $D \sim 7.9 \times 10^{-3}$ C cm^{-2}; (c) $t = 94$ s, $D \sim 2.2 \times 10^{-2}$ C cm^{-2}; (d) $t = 184$ s, $D \sim 4.3 \times 10^{-2}$ C cm^{-2}. Microvoids are indicated by 'V', cracks in the starch-rich phase due to microtoming are indicated by 'M' in (a). Thinner areas are observed adjacent to the starch-rich domains and are most likely due to deformation at the starch-rich/EVOH-rich interface during microtoming. The horizontal line shown in (a) represents the region selected for intensity plots displayed in *Figure 6*

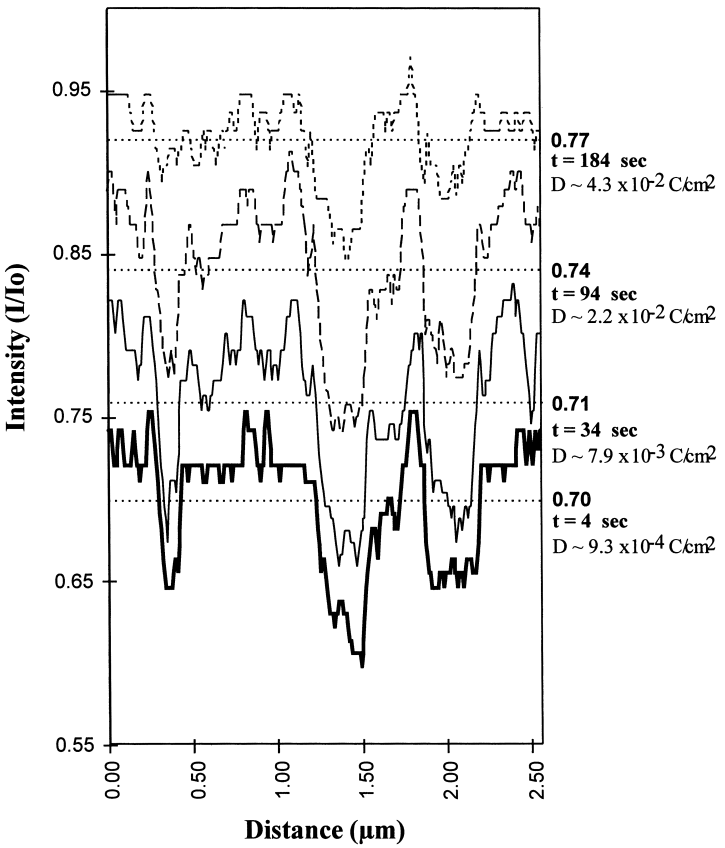

Figure 6 Intensity profiles of an iodine stained NC30 sample as a function of time in the electron beam at a current density of approximately 2.3×10^{-4} A cm^{-2} (at 5 k×). Plots are arbitrarily shifted along the *y* axis to eliminate overlapping of profiles. Note, contrast between the starch-rich and EVOH-rich domains initially increases, then falls as the total beam dosage increases. Average normalized intensities, (I/I_o), total beam exposure time, *t*, and estimated beam dosage, *D*, are shown at the right of the figure

blend shows an increase in the mottling in the matrix and a loss of the light boundary surrounding the starch-rich domains. Overall the average contrast increases slightly ($C = 0.14$) which may be due to the loss of physisorbed iodine from amorphous areas of the EVOH-rich region. *Figure 5c* is similar to the above figure after 90 s of beam exposure although contrast between the starch and EVOH regions begins to decay ($C = 0.12$). After 180 s of beam exposure, contrast between these domains decreases to approximately 0.06 (*Figure 5d*). As the starch-rich regions are irradiated, they undergo loss of crystallinity which would release the complexed iodine and change the mass thickness contrast between the starch- and EVOH-rich regions. Also visible in *Figure 5d* are alternating bands of light and dark grey in the EVOH-rich matrix. These bands (repeating~140 nm) form as different regions in the EVOH-rich matrix are irradiated and are therefore probably not due to the presence of starch-rich domains.

If the microscope is operated at higher magnification, M_2, under the same beam intensity (i.e. such that the optical density of the exposed film is similar for a given fixed exposure time), the specimen dose increases by a factor of $(M_2/M_1)^2$ [31]. *Figures 7* and *8* depict more dramatic contrast changes over a region of the NC30 for micrographs taken under similar conditions as in *Figure 6*, but at the higher magnification of 10 k×. As the sample experiences these moderate doses, the initial contrast measured as 0.08, reduces to zero after only 1 min exposure. Increasing beam dosage results in an inversion of contrast that at 2 min is noticeable ($C = -0.03$) and after 5 min the inverted level of contrast becomes similar to that of the initial image ($C = -0.08$). Imaging these starch-based systems under normal TEM conditions (or at higher magnifications) will cause this contrast reversal to occur sooner and lead to a definite misinterpretation of the blend morphology.

With knowledge of the changes in structure that can occur when starch-EVOH blends are imaged in TEM, the appropriate electron optical conditions are then selected for examining the morphology of starch/EVOH blends comprised of various compositions and starch types. Since more than one structural technique is necessary to fully understand the morphology of this blend system, we only present the type of information which can be gained from TEM in this paper. A more complete discussion with reference to other techniques is presented elsewhere[25].

Compositional influence on the morphology of NC blends

The morphology of the native corn starch and EVOH blends (NC series) that forms following extrusion blending is shown in *Figure 9*. It should be noted that the blends were microtomed nearly perpendicular to the extrusion direction. The morphology shown in *Figure 9a* for the NC15 blend is similar to that observed in more typical phase-separated polymer blends (droplets in a matrix). The starch forms discrete domains which range in diameter from 0.2 to up to 3 μm in an EVOH-rich matrix. Increasing the starch composition to 30% relative to EVOH results in the microstructure observed for the NC30 blend (*Figure 9b*). The size distribution of starch-rich domains is again varied but ranges from less than 0.1 μm to 1.2 μm. The discrete nature of the starch-rich domains is again visible in the NC50 material (and of the same size scale as the NC30 material) although now the area fraction of starch-rich domains is higher and the distance between any two domains is less than 0.5 μm (*Figure 9c*). At a majority composition of the starch component (70% starch, 30% EVOH by weight), the NC70 blend begins to show a complex morphology. The intermaterial dividing surface between the starch-rich and EVOH-rich domains tends to still have positive curvature towards the EVOH component at even up to 70% starch (*Figure 9d*). This structure indicates that the EVOH component is well distributed throughout the blend and continues to act as a matrix component. In the larger dark areas, however, small (~0.25 μm) droplet-like grey inclusions, corresponding to EVOH-rich domains, are visible. This morphology can thus be described as discrete composite domains with starch as the majority component within a minority matrix phase of predominantly EVOH. Finally, as the starch content is increased even further (85% starch to 15% EVOH), light

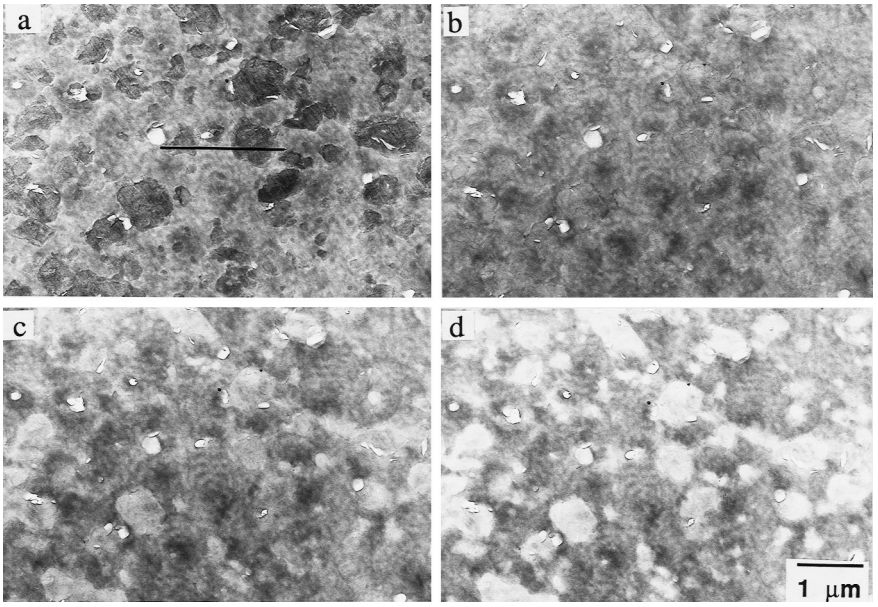

Figure 7 Bright field micrographs showing an iodine stained NC30 blend section as a function of time in the beam at a current density of approximately 2.3×10^{-4} A cm^{-2} (at 5 k×): (a) initial exposure, $t = 4$ s, D~3.7×10^{-3} C cm^{-2}; (b) $t = 64$ s, D~6.0×10^{-2} C cm^{-2}; (c) $t = 124$ s, D~1.1×10^{-1} C cm^{-2}; (d) $t = 304$ s, D~2.8×10^{-1} C cm^{-2}. The line shown in (a) represents the region for intensity plots displayed in *Figure 8*

grey regions less than 0.3 μm in width were observed to be uniformly distributed throughout the NC85 extrudate section (*Figure 9e*). Dark grey domains approximately 0.2–0.5 μm were also observed. This system appeared to be phase separated, but the minority EVOH-rich component forms much smaller and well distributed domains within a mottled starch-rich matrix.

Comparison of blend morphologies for different starch types with EVOH

Extrudate, in the form of pellets, was microtomed perpendicular to the extrusion direction and observed in TEM to discern differences in the phase structure for blends of each starch type. Micrographs were taken of the 50% starch blends, since these are illustrative and provide easy visualization of both the starch and EVOH components. *Figure 10* shows three distinct types of morphology for the three types of 50/50 starch/EVOH blends. As shown in *Figure 10a*, excellent contrast exists between the iodine-stained, starch-rich, dark phase, and EVOH-rich, light phase regions for the Waxy Maize blend (WM50). At 50/50 composition, the EVOH is a continuous phase, starch is discrete. Oriented droplets ranging from 0.05 μm to approximately 5 μm in length were visible with L/D values averaging 1.8 ± 0.5 (smallest droplets are least oriented, as expected). Irregularities in droplet shape and the fact that these droplets exhibited some preferred orientation (when observed in extrudates cut parallel to the extrusion direction) indicates that optimum blending between the two polymer components has not been achieved during the extrusion process[56]. Smaller light phase domains appear within the darker regions indicating the formation of composite droplets. Overall, a very complex, phase separated structure was observed for the WM50 blend[56].

The morphology of the NC50 blend extrudate appears quite different (see *Figure 10b*). Dark, ellipsoidally-shaped domains with major axes of approximately 0.05–1.2 μm were distributed within a lighter matrix. Unlike in the WM50 blend, no composite droplets were observed. The EVOH-rich, lighter area, appeared continuous throughout the sections indicating that this component (or a mixture of mostly EVOH and some of the starch fraction) forms the matrix. Starch-rich domains were visible as discrete domains within this matrix. Although the densities of the waxy maize and native corn starches are similar, the contrast between the starch-rich domains and the blend matrix is lower. This observation may indicate that the amylose fraction in the Native Corn starch may be partially miscible with the EVOH fraction.

Finally, the HY50 blend exhibits a finer dispersion of smaller starch-rich domains distributed throughout a grey matrix (*Figure 10c*). Domain sizes average less than 0.25 μm; however, an accurate determination of domain sizes is difficult due to the number the small and finely dispersed domains. Significant microvoiding is also observed in this material. Overall, the microstructure of HY blends is more difficult to visualize due to the lower initial contrast level between the starch-rich and EVOH-rich domains which quickly fades as the sample is observed in TEM. Since densities of the three starch types are similar (1.45–1.47 g cm^{-3}), the lack of mass thickness contrast differences is strongly suggestive of a partially miscible system.

In *Figure 11*, the variation in observable starch-rich domain sizes for the three different starch/EVOH blend

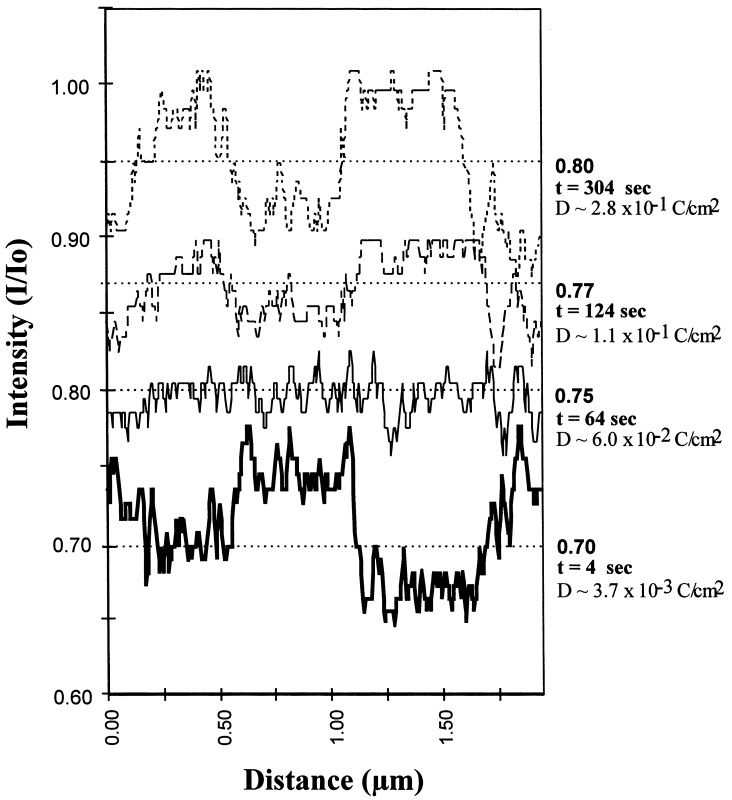

Figure 8 Intensity profiles of an iodine stained NC30 sample as a function of time in the electron beam under similar operating conditions as in *Figure 6*, but at higher magnification (at 10 k×). Plots are arbitrarily shifted along the *y* axis to eliminate overlapping of profiles. Contrast decreases to zero then reverses as the specimen undergoes significant beam damage. Average normalized intensities, (I/I_o), total beam exposure time, *t*, and estimated beam dosage, *D*, are shown at the right of the figure

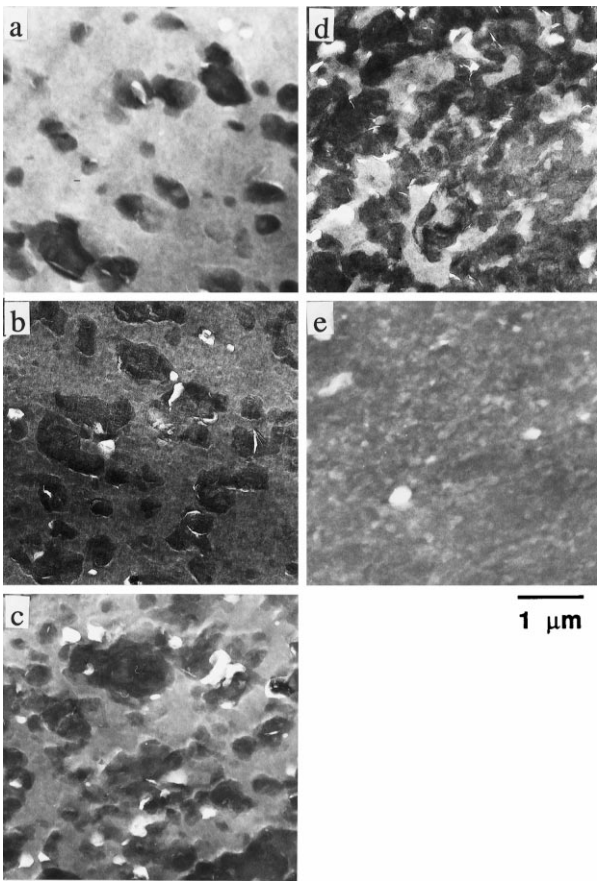

Figure 9 Bright field electron micrographs of representative Native Corn starch/EVOH blends which were stained with iodine: (a) NC15, (b) NC30, (c) NC50, (d) NC70, and (e) NC85. EVOH appears to be the matrix component even at high compositions (up to 70%) starch. Total dose per image is estimated to be less than 1×10^{-3} C cm^{-2}

types is presented graphically. The values shown are estimated from various TEM and SEM micrographs. Overall, the starch-rich domain sizes are largest for the Waxy-Maize (WM) blends, and the transition to a continuous starch-rich matrix takes place at a much higher loading level ($>$ 70 wt.% WM). Native corn starch/EVOH (NC) blends also exhibit a range of starch-rich domain sizes. The starch-rich phase becomes continuous for blends containing between 50 and 70 wt.% starch. At low starch levels of the NC and WM blends ($<$ 30 wt.% starch), the starch-rich domains actually increase in size. At these compositions, the starch granules may experience reduced shear forces in the lower viscosity EVOH-rich matrix, which could result in coarser destructurization. Starch-rich domain sizes for the HY blends are estimated to be less than 0.25 μm. When a starch-rich matrix forms, a partially miscible Hylon VII/EVOH blend can be hypothesized. Further work is necessary to fully characterize the phase behaviour of these blends.

Cross-sectional TEM of a starch/EVOH fibre

TEM is also useful in examining structural differences that might occur due to subsequent processing such as fibre spinning. The near surface region of an NC50 melt spun monofilament[2] is shown in *Figure 12*. The diameter of this fibre is 175 μm with a draw ratio of 20. After drying the filament in a desiccator for 24 h, the fibre was embedded in epoxy, and microtomed perpendicular to the draw direction. Sections were then stained for 1 h with iodine. The dark region appearing on the top left corner of the micrograph is the epoxy, a knife mark is visible as a diagonal line near the top edge of the fibre. A gradient structure is visible at the fibre surface as evident by the light band approximately 1 μm wide that traces the surface of the fibre, this light band becomes progressively darker as it approaches the interior of the fibre. This peripheral region is predominantly unstained EVOH. A number of inclusions ranging in size from less than 0.1 μm to approximately 0.5 μm are also visible in the micrograph which are starch-rich areas. The lightest areas evident in the micrograph correspond to microvoids.

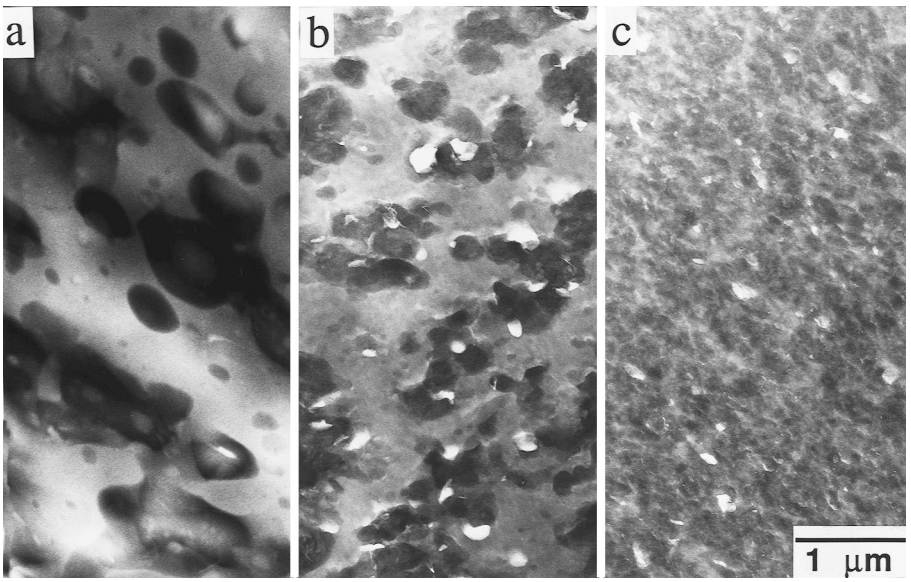

Figure 10 Bright field electron micrographs showing the effect of starch type on the blend morphology for 50:50 starch/EVOH compositions: (a) Waxy Maize (WM50), (b) Native Corn (NC50), and (c) Hylon VII (HY50) blends. As the amylose content of the starch component increases, the starch-rich domain sizes decrease and contrast between starch-rich and EVOH-rich regions decreases

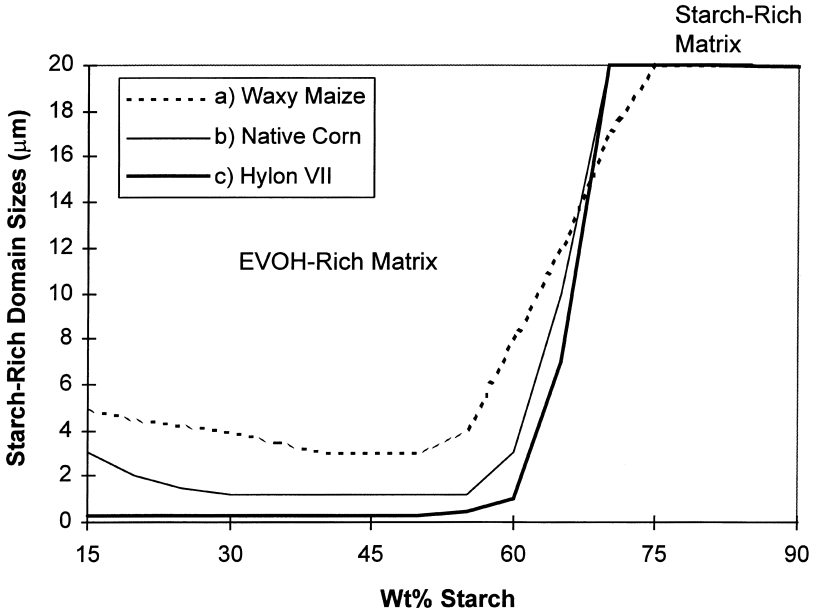

Figure 11 Variation in observed phase sizes as a function of composition for the three starch/EVOH blend series: (a) Waxy Maize (WM), (b) Native Corn (NC), and (c) Hylon VII (HY). The values shown are estimated from various TEM and SEM micrographs

The EVOH-rich surface layer on the fibre can be explained by considering the fibre spinning process of blends containing components of different melt viscosities. As the lower viscosity component in the melt, the EVOH fraction becomes more concentrated nearer to the walls of the spinneret capillary, which are the regions of highest shear strain. When the fibre is drawn, EVOH is still present near the surface but a roughness develops due to the presence of the starch fractions which have a low elongational viscosity and limit the overall draw properties (and hence, final diameter) of the fibre. This surface structure has been confirmed by the enzymatic etching of the fibres and observation in SEM. The starch-rich domains are etched away in the interior of the fibre but the surface of the fibre is not affected. This structural information is essential in interpreting biodegradability and transport properties since degradation and diffusion will be retarded at the EVOH-rich surface of the fibre. Further details of this work are presented and discussed separately[2].

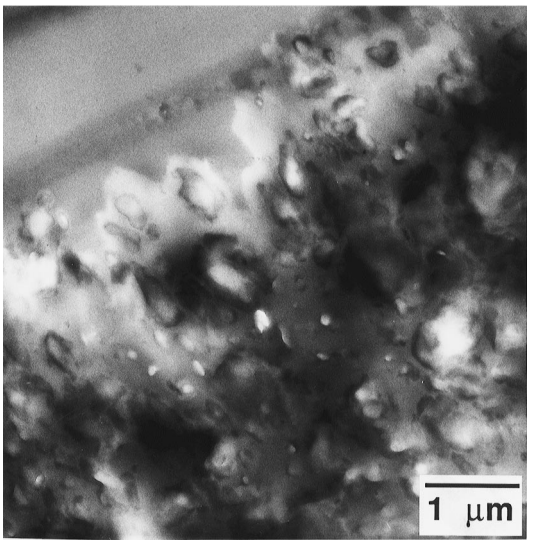

Figure 12 Bright field electron micrograph showing the near surface region of a Native Corn starch/EVOH fibre (NC50). The fibre was embedded in epoxy and stained with iodine vapour. The epoxy appears in the left upper region of the micrograph. The light EVOH component is more concentrated at the fibre surface

CONCLUSIONS

The morphologies of complex thermoplastic systems, starch/poly(ethylene-vinyl alcohol) (EVOH) blends, were investigated using a conventional transmission electron microscope. Using the optimum sample preparation and imaging conditions, the average size and distribution of domains for starch/EVOH blends was observed to change as the starch content was varied. EVOH was found to be the matrix component even at very high starch concentrations (up to 70%). Differences in the blend structure were also observed at similar starch compositions for three corn starch varieties. Blends containing amylose appeared to be at least partially miscible based on contrast differences between the WM, NC, and HY blend series. Microvoiding of plasticizer during the extrusion blending process was also evident at the periphery of starch-rich regions. Finally, by using cross-sectional TEM, the concentration of EVOH was found to be higher at the surface of a melt-spun starch/EVOH fibre.

The structural changes that occurred to the respective blend components were monitored as a function of beam dose. At 200 keV and 20°C, maximum allowable beam dosage for starch was noticeably less than 3×10^{-3} C cm^{-2} and for EVOH, approximately 3.5×10^{-3} C cm^{-2}. Although a small amount of image contrast was observed in the Native Corn starch/EVOH blend ($C = 0.05$), it was more than doubly enhanced through the use of iodine to preferentially stain the starch fraction. For the starch/EVOH system, contrast initially increased then decreased as the sample was further exposed to the electron beam. At moderate electron beam dosages greater than 6×10^{-3} C cm^{-2}, contrast reversal between the starch-rich and EVOH-rich regions occurred. This functional dependence of contrast differences requires that beam dose be monitored as starch/EVOH blends are imaged.

Otherwise, the actual morphology may be easily misinterpreted (e.g. for a 50/50 starch/EVOH blend).

ACKNOWLEDGEMENTS

The authors would like to thank Novon Products, Warner-Lambert Corp. for providing materials and assistance in making the blends. Acknowledgment is made to the Center for Materials Science and Engineering at MIT for use of its electron microscope facility.Funding was provided by the U.S. Dept. of Agriculture, (grant # 91-COOP-2-6108). SS also acknowledges the National Science Foundation for providing a graduate fellowship.

REFERENCES

1. Thomas, E. L., Transmission electron microscopy of polymers, in *Structure of Crystalline Polymers*, ed. I. H. Hall. Elsevier Applied Science Publishers, New York, 1984, p. 79.
2. Simmons, S. Ph.D. Thesis, Massachusetts Institute of Technology, 1995.
3. Lay, G., Rehm, J., Stepto, R. F., Thoma, M., Sachetto, J.-P., Lentz, D. J. and Silbiger, J., US Patent No. 5095054, Warner-Lambert Company, 1992.
4. Bastioli, C., Lombi, R., Del Tredici, G. and Guanella, I., Eur. Patent Application, 90110070.1, Butterfly S.R.I., 1990.
5. Dell, P.A. and Kohlman, W.G., *Journal of Applied Polymer Science*, 1994, **52**, 353.
6. Gallant, D. and Guilbot, A., *Die Staerke*, 1969, **21**, 156.
7. Chabot, J.F., Allen, J.E. and Hood, L.F., *Journal of Food Science*, 1978, **43**, 727.
8. Yamaguchi, M., Kainuma, K. and French, D., *J. Ultrastructural Research*, 1979, **69**, 249.
9. Guilbot, A. and Mercer, C., Starch, in *The Polysaccharides*, ed. G. O. Aspinall. Academic Press, New York, 1985.
10. Kanenega, K., Koreeda, A., Harada, A., Okuyama, K. and Harada, T., *Chemistry Express*, 1989, **12**, 781.
11. Buttrose, M. S., *J. Ultrastructural Research*, 1960, **4**, 241.
12. Buttrose, M. S., *Die Staerke*, 1963, **15**, 85.
13. Whistler, R. I. and Turner, E. S., *J. Poly. Sci. (Letters)*, 1944, **18**, 153.
14. Mussulman, W. C. and Wagoner, J. A., *Cereal Chemistry*, 1968, **45**, 162.
15. Kassenbeck, P., *Die Staerke*, 1975, **27**, 217.
16. Kassenbeck, P., *Starch/Staerke*, 1978, **30**, 40.
17. Gallant, D. J. and Sterling, C., Electron microscopy of starch and starch products, in *Examination and Analysis of Starch and Starch Products*, ed. J. A. Radley. Applied Science Publishers, London, 1975.
18. Blanshard, J. M. V., Starch granule structure and function: a physiochemical approach, in *Starch: Properties and Potential*, ed. T. Galliard. Wiley, New York, 1987.
19. Chanzy, H., Vuong, R. and Jesior, J. C., *Starch/Staerke*, 1990, **42**, 377.
20. Banks, W. and Greenwood, C. T., in *Starch and Its Components*. Edinburgh University Press, Edinburgh, UK, 1975.
21. Booy, F.P. and Chanzy, H., *Biopolymers*, 1979, **28**, 293.
22. Welland, E. L. and Donald, A. M., *Int. J. Biol. Macromol.*, 1991, **13**, 69.
23. Gohil, R. M. and Patel, R. D., *Die Staerke*, 1976, **28**, 293.
24. Trimmell, D., Swanson, L. and Shogren, R. L., *J. Appl. Polym. Sci.*, 1993, **48**, 1665.
25. Simmons, S. and Thomas, E. L., *J. Appl. Polym. Sci.*, 1995, **58**, 2259.
26. George, E. R., Sullivan, T. M. and Park, E. H., *Polymer Engineering and Science*, 1994, **34**, 17.
27. Thomas, E. L., Electron microscopy, in *Encyclopedia of Polymer Science and Engineering*. Wiley, New York, 1986, p. 644.
28. Roche, E. J. and Thomas, E. L., *Polymer*, 1981, **22**, 333.
29. Zeleznak, K. J. and Hoseney, R. C., *Cereal Chemistry*, 1987, **64**, 121.
30. Reid, N. and Beesley, J. E., *Sectioning and Cryosectioning for Electron Microscopy*. Elsevier Science, New York, 1991.
31. Misell, D. L., *Image Analysis, Enhancement, and Interpretation*. North-Holland Publishing Company, New York, 1978.
32. Thomas, E. L., Electron microscopy of radiation sensitive polymers, in *Developments in Electron Microscopy and Analysis*, ed. J. A. Venables. Academic Press, New York, 1975.
33. Adams, W. W., Ph.D. Dissertation, University of Massachusetts, 1984.
34. Reimer, L., *Laboratory Investigation*, 1965, **14**, 344.
35. Keller, A., Radiation effects and crystallinity in PE and paraffins, in *Developments in Crystalline Polymers — I*, ed. D. C. Bassett. Applied Science Publishers, Englewood, NJ, 1982, p. 37.
36. Hansen, K., in *Advances in Optical and Electron Microscopy— Vol. 4*, ed. R. Barer and V. E. Cosslett. Academic Press, London, 1971.
37. Erickson, H. P., in *Advances in Optical and Electron Microscopy — Vol. 5*, ed. R. Barer and V. E. Cosslett. Academic Press, London, 1973.
38. Chacko, V. P., Adams, W. W. and Thomas, E. L., *Journal of Materials Science*, 1983, **18**, 1999.
39. Vainshtein, B. K., Feigl, E. and Spink, J. A., ed., in *Structure Analysis by Electron Diffraction.* Pergamon Press, Oxford, UK, 1964.
40. Matsumoto, T., Nakamae, K., Ogoshi, N., Kawasoe, M. and Oka, H., *Kobunshi Kagaku*, 1971, **28**, 610.
41. Buleon, A., Delangli, M. M., Brisson, J. and Chanzy, H., *Int. J. Biol. Macromol.*, 1990, **12**, 25.
42. Kanzawa, Y., Koreeda, A., Harada, T. and Harada, T., *Agricultural Biological Chemistry*, 1989, **53**, 979.
43. Kanenaga, K., Kako, K., Harada, T., Koreeda, A., Harada, A. and Okuyama, K., *Chemistry Express*, 1989, **4**, 519.
44. Dombrowski, R., Novon Products, personal communication, 1992.
45. Murano, E., Paoletti, S., Cesaro, A. and Rizzo, R., *Analytical Biochemistry*, 1990, **187**, 120.
46. Reimann, B., *Mikroscopie*, 1961, **16**, 224.
47. Sawyer, L. C. and Grubb, D. T., in *Polymer Microscopy*. Chapman and Hall, New York, 1987.
48. Noltemeyer, M. and Saenger, W., *Nature*, 1976, **259**, 629.
49. Hirai, T., Hirai, M., Hayashi, S. and Ueki, T., *Macromolecules*, 1992, **25**, 6699.
50. Hirai, M., Hirai, T. and Ueki, T., *Polymer*, 1994, **35**, 2222.
51. Takamiya, H., Tanahasi, Y., Matsuyama, T., Tanigami, T., Yamaura, K. and Matsuzawa, S., *Journal of Applied Polymer Science*, 1993, **50**, 1807.
52. Choi, Y.-S. and Miyasaka, K., *Polymer Journal*, 1991, **23**, 977.
53. Choi, Y.-S. and Miyasaka, K., *Journal of Applied Polymer Science*, 1993, **48**, 313.
54. Choi, Y.-S. and Miyasaka, K., *Journal of Applied Polymer Science*, 1994, **51**, 613.
55. Yokota, T. and Kimura, Y., *Makromol. Chem.*, 1993, **194**, 295.
56. Paul, D. R. and Newmann, S., in *Polymer Blends.* Academic Press, New York, 1978.